JCTC Journal of Chemical Theory and Computation

Simulating Monovalent and Divalent Ions in Aqueous Solution Using a Drude Polarizable Force Field

Haibo Yu,[†,‡] Troy W. Whitfield,[‡,§,#] Edward Harder,[†] Guillaume Lamoureux,[||]
Igor Vorobyov,[⊥,∇] Victor M. Anisimov,[⊥] Alexander D. MacKerell, Jr.,[⊥] and
Benoît Roux*[,†,§]

*Department of Biochemistry and Molecular Biology, The University of Chicago, 929
East 57th Street, Chicago, Illinois 60637, Biosciences Division, Argonne National
Laboratory, 9700 South Cass Avenue, Argonne, Illinois 60649, Department of
Chemistry and Biochemistry, Concordia University, Montréal, Québec, H4B 1R6,
Canada, and Department of Pharmaceutical Sciences, School of Pharmacy, University
of Maryland, Baltimore, Maryland 21201*

Received October 29, 2009

Abstract: An accurate representation of ion solvation in aqueous solution is critical for meaningful computer simulations of a broad range of physical and biological processes. Polarizable models based on classical Drude oscillators are introduced and parametrized for a large set of monatomic ions including cations of the alkali metals (Li^+, Na^+, K^+, Rb^+, and Cs^+) and alkaline earth elements (Mg^{2+}, Ca^{2+}, Sr^{2+}, and Ba^{2+}) along with Zn^{2+} and halide anions (F^-, Cl^-, Br^-, and I^-). The models are parametrized, in conjunction with the polarizable SWM4-NDP water model [Lamoureux et al. *Chem. Phys. Lett.* **2006,** *418,* 245], to be consistent with a wide assortment of experimentally measured aqueous bulk thermodynamic properties and the energetics of small ion–water clusters. Structural and dynamic properties of the resulting ion models in aqueous solutions at infinite dilution are presented.

1. Introduction

Ions are fundamental to the structure and function of biological systems, where their local environment can be as diverse as are the roles that they play. Ions are involved in the folding of proteins and nucleic acids, enzyme catalysis, and numerous cellular signaling processes. Monovalent ions such as Na^+, K^+, and Cl^- play an important role in the homeostasis and electric activity of living cells and in modulating biomolecular stability through both specific and nonspecific interactions.[1,2] Divalent cations, such as Zn^{2+}, Mg^{2+}, and Ca^{2+}, are often associated with catalytic or regulatory activities of proteins and enzymes,[3,4] including the activation by Ca^{2+} of K^+ channels,[5] the stabilization by Zn^{2+} of zinc-finger proteins,[6] and the condensation and folding of RNA and DNA by Mg^{2+}.[7−12]

In order to have meaningful computational models to probe and explore the diverse and important roles of ions in biological phenomena, accurate and physically realistic descriptions of their microscopic interactions is crucial. This is not trivial because a balanced description of the interactions between ion and ion, ion and water, and ion and biomolecules is required. A number of nonpolarizable models for ions have been developed.[13−18] The influence of induced electronic polarization, in particular, has been shown to be critical to the study of ion channels,[19−21] and it is expected to be generally important for the study of aqueous ionic systems. Striking a balance between accuracy and computational expense is an important consideration in designing useful models. Because proper statistical averaging in biological

* Corresponding author e-mail: roux@uchicago.edu.
† The University of Chicago.
§ Argonne National Laboratory.
|| Condordia University.
⊥ University of Maryland.
‡ These authors contributed equally to this paper.
# Current address: Program in Bioinformatics and Integrative Biology, University of Massachusetts Medical School, Worcestor, Massachusetts 01605.
∇ Current address: Department of Chemistry, University of California, Davis, California 95616.

Simulating Monovalent and Divalent Ions

J. Chem. Theory Comput., Vol. 6, No. 3, 2010 **775**

systems requires long simulations to sample over many configurations,[22] achieving a sufficient sampling of the relevant configurations can become computationally prohibitive if the microscopic interactions are generated via sophisticated ab initio quantum mechanical (QM) approaches. In that regard, treatments of many-body polarization effects based on simple potential functions have important advantages over QM methods. An alternative approach is to adopt a polarizable force field.[23−26]

Generally speaking, there are three different methods to account for explicit electronic polarization into classical force fields, i.e., induced dipole model, fluctuation charge model, and classical Drude oscillator model. Correspondingly, a number of polarizable models for ions have been developed based on these three different approaches to study a variety of phenomena involving ions.[27−30] Our own efforts have been focused on developing a complete all-atomic polarizable force field for proteins, nucleic acids, and membranes based on the concept of the classical Drude oscillator.[31] This model approximates the quantum mechanical electronic responses by using auxiliary massless charged particles that are harmonically bound to the polarizable nuclei.[24,26,29,32−35] This approach is also referred to as the "shell model"[36−38] or "charge-on-spring".[24,39] The polarizable Drude force field has been shown in previous studies to be accurate for the simulation of liquid water,[33−35] aqueous ionic systems,[29] condensed phases of small organic molecules,[40−44] and lipid membranes.[45] In these efforts, all new chemical entities must be compatible with the polarizable SWM4-NDP water model,[35] which serves as the central reference for the polarizable Drude force field.

In the present paper, models for an extended set of ions are constructed and parametrized to be compatible with the SWM4-NDP water model.[35] The set comprises the most abundant and biologically relevant monatomic ions, including cations of the alkali metals (Li^+, Na^+, K^+, Rb^+, and Cs^+) and alkaline earth elements (Mg^{2+}, Ca^{2+}, Sr^{2+}, and Ba^{2+}) along with Zn^{2+} and halide anions (F^-, Cl^-, Br^-, and I^-). The present models of alkali and halide ions are similar to those developed previously,[29] which were parametrized in conjunction with the SWM4-DP water model.[34]

Because the SWM4-DP and SWM4-NDP models differ in the sign of the charge on the auxiliary Drude particle attached to the oxygen atom, a reparametrization is necessary to have models compatible with the SWM4-NDP water model.[35] In addition, models for divalent cations are introduced and parametrized. The latter pose new challenges for a classical polarizable force field, particularly regarding the treatment of overpolarization and Coulombic singularities. Approaches to overcome these problems are presented.

The paper is organized as follows. Section 2 recapitulates the relevant details of the Drude model for ion solvation and articulates the questions that arise when extending it to treat highly polarizable anions and divalent ions, along with steps that have been taken to solve the problem. Also included in section 2 are the parametrization strategy and target data. In section 3, results of the fitting are presented for our set of ions, along with an analysis of the structural properties and polarization effects that are predicted by the model.

2. Theory and Methods

2.1. Classical Drude Polarizable Model. The model ions are consistent with the SWM4-NDP polarizable water model with a negatively charged Drude oscillator bound to its oxygen site.[35] The SWM4-NDP potential reproduces most properties of bulk water under ambient conditions (density, vaporization enthalpy, radial distribution function, dielectric constant, self-diffusion constant, shear viscosity, and free energy of hydration). In particular, the SWM4-NDP model yields a correct static dielectric constant, which makes it appropriate to study systems dominated by water-mediated electrostatic interactions. The SWM4-NDP water model comprises five interaction sites: (1) the oxygen atom "O" carrying a charge of $-q_D^{wat}$, (2) the Drude particle "D" harmonically attached to the oxygen atom carrying a (negative) charge of q_D^{wat}, (3) the massless auxiliary site "M" carrying a charge q_M^{wat}, and (4 and 5) the hydrogen atoms "H_1" and "H_2", each carrying a charge of q_H^{wat}. The interactions within and between water molecules are calculated according to the formulation of the polarizable Drude model described in refs 33 and 34. The ion models comprise two sites: (1) the ion core atom "A" carrying a charge of $q^{ion} - q_D^{ion}$ and (2) a Drude particle "D" attached to the ion atom carrying a (negative) charge of q_D^{ion}. To be consistent with the SWM4-NDP model, polarization of an ion is represented by a negatively charged particle, representing electron density, bound to its nucleus (core). All atomic dispersion and electronic overlap effects are represented in a pairwise additive way using the Lennard−Jones (LJ) potential. The core repulsion and van der Waals dispersive interactions are modeled by a LJ interaction between the water oxygen and the ion core atom via the Lorentz−Berthelot combination rule.[46] The potential energy of one ion and one water molecule can be written as

$$U_{tot}^{iw} = U_{LJ}^{iw} + U_{Drude}^{iw} + U_{elec}^{iw} \qquad (1)$$

where U_{LJ}^{iw} is the LJ interaction between the ion and the water oxygen atom, U_{Drude}^{iw} represents the harmonic restoring springs associated with the Drude oscillator of the water molecule and the ion, and U_{elec}^{iw} includes all the Coulombic electrostatic interactions between the fixed and mobile charges carried by the ion (two sites) and the water molecule (five sites). The spring constant K_D is set to 1000 kcal/mol/Å^2 for all Drude oscillators in the system. This value dictates the magnitude of the charge that the Drude particle must carry to produce the correct polarizability α, i.e., $q_D = -(\alpha K_D)^{1/2}$.[35] For example, the charge on the Drude particle of I^-, the most polarizable ion in the current study, is − 4.733e with this restoring spring constant.

Simulations of the models are performed by considering the dynamics of an extended Lagrangian in which a small mass m_D and kinetic energy are attributed to the Drude particles. The amplitude of the Drude oscillators is controlled with a low-temperature thermostat acting in the local center-of-mass reference frame of each atom−Drude pair.[33] The mass of the Drude particles is set to 0.4 amu, which is subtracted from the mass of the physical polarizable nucleus such that the total mass of the pair remains constant. To

ensure that the time course of the induced dipoles stays close to the self-consistent field (SCF) solution, a Nosé–Hoover thermostat at a temperature $T_* = 1$ K is applied to the relative motion of each atom–Drude pair (in their local center-of-mass reference frame). It was shown that the trajectories generated according to this procedure are very close to those generated by the SCF regime of induced polarization.[33,34] To control the global thermalization of the system, a second thermostat is applied to the center of mass of the atom–Drude pairs as well as the hydrogen atoms.

2.2. Overpolarization of Drude Oscillators. The simple sum over Coulomb interactions of U_{elec} in eq 1 does not exclude singular r^{-1} attractive interactions between the Drude particles and other interaction sites carrying a net charge. Such singularities are generally not problematic in fixed-charge force fields, where the charges are buried within r^{-12} LJ core repulsive interactions. In the polarizable model based upon the Drude oscillator, however, the charge on the Drude particles is not as effectively shielded from other charges by such nonelectrostatic core repulsive interactions. To clarify the situation leading to singularities, consider the interaction between a Drude oscillator bound to a heavy atom fixed at the origin and a point charge q_i placed at some distance X. Along the one-dimensional axis, the potential energy is

$$U(x) = \frac{1}{2}K_D x^2 + \frac{q_D q_i}{|X|} - \frac{q_D q_i}{|X - x|} \quad (2)$$

where x is the displacement of the oscillator, q_D is the magnitude of the charge on each end of the Drude oscillator, and K_D is the harmonic restoring force constant. The self-consistent field condition is

$$\frac{dU(x)}{dx} = K_D x - \frac{q_D q_i (X - x)}{|X - x|^3} = 0 \quad (3)$$

The point of inflection for this solution becomes unstable when

$$X = \left(\frac{27}{4}q_i\sqrt{\frac{\alpha}{K_D}}\right)^{1/3} \quad (4)$$

at which point $x = X/3$. For a fixed value of K_D, instabilities can occur when the polarizability α is large, as in the case of some anions, or when the charge q_i is large, as in the case of the small monatomic divalent cations.

To illustrate the instabilities encountered with a divalent cation ($q_i = 2.0e$), we substitute the charge and force constant parameters from the SWM4-NDP water model. The results are illustrated in Figure 1. Substituting parameters for the SWM4-NDP water model into eq 4, one finds that $X = 1.974$ Å. For example, when the divalent cation is placed at a distance of $2X$ from the origin, the Drude particle can reside in a stable minimum located at $x \approx 0.14$ Å (Figure 1). However, as shown in Figure 1, placing the divalent cation $X < 1.974$ Å will cause the SWM4-NDP oscillator to fall into the singular Coulomb well at X. In contrast, the system is stable with a monovalent cation ($q_i = 1.0e$): according to eq 4, the instability appears only at $X = 1.567$ Å.[29] This distance is considerably shorter than that observed for ion–water close contacts in simulation of ions in solution.
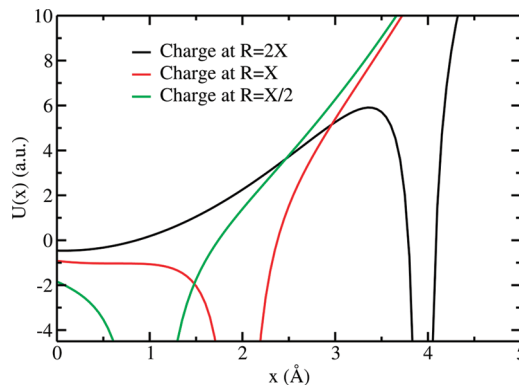

Figure 1. SWM4-NDP water molecule with a point charge of $+2e$ placed $2X$, X, and $X/2$ defined by eq 4 away from the oxygen atom.

Monovalent cations, unlike those for the divalent cations with the oxygen Drude sites on SWM4-NDP water molecules, therefore need no special treatment in order to avoid the "polarization catastrophe".[29]

A number of empirical remedies to the overpolarization problems are possible. The simplest treatment is to introduce an additional anharmonic restoring force to prevent excessively large excursions of the Drude particle away from the atom.[39] The value of such anharmonic term can be adjusted to reduce the polarizability of atoms at high field. This approach was used to prevent any instabilities with the highly polarizable anions such as Br^- and I^-. The anharmonic restoring force was chosen to be active only beyond a certain stretching distance ΔR_{cut}

$$U_{hyp} = K_{hyp} \cdot (\Delta R - \Delta R_{cut})^4 \quad (5)$$

thus preserving the linear polarization response with small displacements.

The cutoff was chosen to be based on the maximum displacement of the Drude particles with respect to their nuclei in SWM4-NDP water models to ensure that its properties will not be affected. The force constant was chosen to be 40 000 kcal/mol/Å^4 to reproduce the maximum induced dipole moment of halide anions estimated by MP2 calculations (see Supporting Information Figure S1). If the stiff anharmonic restoring force causes numerical instability with the finite time-step integrator, the problem could be treated using a multiple time-step algorithm, where the rapidly varying restoring forces are integrated with a smaller time step than the remaining slowly varying forces.[47]

A second possibility is to associate a small repulsive core to the Drude particle implemented with the NBFIX option in the program CHARMM.[48] Finally, another possibility is to introduce electrostatic screening functions that alter the charge–charge $1/r$ Coulombic interactions at short distances.[30,49–52] The latter approach was used to construct stable and accurate models of the divalent cations. A screening function was introduced to modulate the electrostatic interactions between the divalent ion and the induced dipole component of the oxygen of the water molecules

Simulating Monovalent and Divalent Ions

J. Chem. Theory Comput., Vol. 6, No. 3, 2010 **777**

$$\frac{q_i q_j}{r_{ij}} \rightarrow \left(\frac{q_i q_j}{r_{ij}} \right) S_{iw}(r_{ij}) \tag{6}$$

where r_{ij} are the distances between the pairs of charges taken from $q_i = \{q^{ion} - q_D^{ion}, q_D^{ion}\}$ and $q_j = \{-q_D^{wat}, q_D^{wat}\}$. The screening function $S_{iw}(r)$ is given by

$$S_{iw}(r) = 1 - \left(1 + \frac{r}{2a_{iw}} \right) e^{-r/a_{iw}} \tag{7}$$

where $a_{iw} = (\alpha_i \alpha_w)^{(1/6)}/t_{iw}$ and α_i and α_w are the polarizabilities of the ion and oxygen of the water molecule, respectively. This functional form of electrostatic screening was originally introduced for point dipoles by Thole.[40] The dimensionless Thole parameter t_{iw} modulates the strength of the screening for the ij pair. In the polarizable Drude model, this form has previously been utilized to modulate the intramolecular nearest-bonded-neighbor 1−2 interactions and next-nearest-bonded-neighbor 1−3 interactions.[43] For the divalent cations, the four terms representing the electrostatic interactions between the ion−Drude pair and the water oxygen−Drude pair were treated using eq 7.

2.3. Free Energy Calculations. The absolute hydration free energy of the ions was calculated and decomposed into three contributions following a free energy perturbation simulation protocol established previously[29,53]

$$\Delta G_{hydr} = \Delta G_{rep} + \Delta G_{disp} + \Delta G_{elec} \tag{8}$$

where ΔG_{rep} and ΔG_{disp} are the repulsive and attractive (dispersive) components, respectively, of the LJ interaction in eq 1. The electrostatic component of the hydration free energy is ΔG_{elec}. Each component of the total hydration free energy was computed from independent simulations in which an ion was placed in a periodic box containing 216 explicit SWM4-NDP water molecules. Long-range electrostatic interactions were computed using particle mesh Ewald summation.[54] A smooth real-space cutoff is applied between 10 and 12 Å with an Ewald splitting parameter of 0.34 Å^{-1}, a grid spacing of ∼1.0 Å, and a sixth-order interpolation of the charge to the grid. The isothermal−isobaric ensemble was simulated using a Nosé−Hoover thermostat[55,56] and the modified Andersen−Hoover barostat of Martyna et al.[57] along with a 1 fs time step. The internal geometry of the SWM4-NDP water molecule was kept rigidly fixed using the SHAKE/Roll and RATTLE/Roll algorithm.[58,59] For each value of the thermodynamic coupling parameter, λ, after an initial equilibration of 200 ps, equilibrium properties were averaged over a 400 ps molecular dynamics simulation. For the dispersive and electrostatic components, λ took on values between $\lambda = 0$ and $\lambda = 1$ that were evenly spaced in increments of 0.1. For the repulsive term, λ took on the following values: 0, 0.05, 0.1, 0.15, 0.2, 0.25, 0, 3, 0.35, 0.4, 0.5, 0.6, 0.7, 0.8, 0.9, 1. The repulsive contribution, ΔG_{rep}, was computed using a soft-core scheme as described elsewhere[53] and unbiased using the weighted histogram analysis method (WHAM),[60] while ΔG_{disp} and ΔG_{elec} were computed using thermodynamic integration (TI). On the basis of multiple runs, the overall precision of the calculated absolute hydration free energies with the current protocol is on the order of 0.2 kcal/mol for monovalent ions and 0.5 kcal/mol for divalent ions.

In discussions of the hydration free energy of ionic species, one may consider the *real* physical value, which includes the contribution of the phase potential arising from crossing the physical air/water interface or the *intrinsic* bulk phase value, which is independent of the interfacial potential.[29,61,62] The relationship between *real* and *intrinsic* hydration free energies is defined as $\Delta G_{hydr}^{real} = \Delta G_{hydr}^{intr} + zF\Phi$, where F is the Faraday constant (23.06 kcal/mol/V) and Φ is the electrostatic Galvani potential at the liquid−vacuum interface or the phase potential of the liquid relative to vacuum. It may be tempting to consider the intrinsic free energy as somehow reflecting more faithfully the true hydration free energy of the ion within the bulk phase because it is "disentangled" from the bias arising from the liquid−vacuum interfacial potential. However, it should be noted that the actual value of Φ depends upon the convention to define the Galvani potential. One may construct an "internal" Galvani potential via a P-sum, where the potential at all points in space is the superposition of the total charge density from all the particles.[63,64] Alternatively, one may construct an "external" Galvani potential via a M-sum, where the potential from each water molecule contributes only to points in space that are outside their repulsive core.[63,64] Although the internal or external Galvani potentials can be defined mathematically without ambiguity by specifying which P- or M-sum convention has been used, they cannot be measured experimentally by a physical process.

To avoid any ambiguity, only *real* hydration free energies are considered throughout the present study. ΔG_{hydr}^{real} corresponds to the reversible thermodynamic work to move a single ion from vacuum to the interior of a pure water phase (i.e., across the physical liquid−vacuum interface). Our free energy calculations with periodic boundary conditions (PBC) and particle mesh Ewald are carried out within the P-sum convention, and the implicit reference phase potential of the liquid is the "internal" Galvani potential. Such free energy calculations yield ΔG_{hydr}^{intr}, which then needs to be shifted by $z\Phi$ (calculated within the same P-sum convention) to yield the physically meaningful ΔG_{hydr}^{real}. For our polarizable SWM4-NDP water model, the P-sum internal Galvani potential Φ is equal to -545 mV[35] (negative in the liquid phase relative to vacuum), giving rise to an energy shift of ∓ 12.6 kcal/mol for the monovalent cations/anions and twice that amount for the divalent species. Finally, for a direct comparison with published experimental tables, it is necessary to convert the results into the free energy of an ion going from an ideal gas at 1 atm to an idealized bulk solution at 1 M concentration. To account for the compression from a volume of 24.465 L/mol in the ideal gas to the 1 M solution, a small entropic contribution of $-k_B T \ln (1/24.465) = 1.9$ kcal/mol must be added per ion.[29]

2.4. Target Data and Parametrization Strategy. *2.4.1. Ionic Charges and Polarizabilities.* For the alkali cations and halide anions, the values of the polarizabilities from the earlier parametrization compatible with the SWM-DP water model were used here without changes.[29] In Table 1 included among these polarizabilities are gas-phase values,

Table 1. Parameters for Alkali Cations, Halide Anions, and Divalent Cations with Negatively Charged Drude Oscillators

	q (lel)	α (Å^3)[a]	$-q_D$ (lel)	E_{min} (kcal/mol)	$R_{min}/2$ (Å)	Thole t_{iw}
Li$^+$	+1	0.032 (0.032)	0.310427	0.0300000	1.1000000	
Na$^+$	+1	0.157 (0.157)	0.687597	0.0315100	1.4616800	
K$^+$	+1	0.830 (0.830)	1.580968	0.1419265	1.6866521	
Rb$^+$	+1	1.370 (1.370)	2.031161	0.2730669	1.7855083	
Cs$^+$	+1	2.360 (2.360)	2.665877	0.2766036	2.0238218	
F$^-$	−1	1.786 (2.467)	2.319199	0.0026181	2.4622406	
Cl$^-$	−1	3.969 (5.482)	3.457187	0.0719737	2.4811139	
Br$^-$	−1	5.262 (7.268)	3.980713	0.0823440	2.6262883	
I$^-$	−1	7.439 (10.275)	4.733085	0.2084343	2.7579694	
Zn^{2+}	+2	0.420 (0.420)	1.124637	0.2500000	0.9349678	2.14773
Mg^{2+}	+2	0.075 (0.075)	0.475246	0.0500000	1.1264156	1.51567
Ca^{2+}	+2	0.490 (0.490)	1.214747	0.2100000	1.2708552	1.50877
Sr^{2+}	+2	0.870 (0.870)	1.618629	0.3400000	1.3059400	1.23792
Ba^{2+}	+2	1.560 (1.560)	2.167454	0.6000000	1.5717385	1.45869

[a] In parentheses are the ab initio estimates of the gas-phase polarizabilities from which the values for α are derived (see ref 65 for the alkali ions and ref 66 for the halide ions and divalent ions).

Table 2. Properties of Alkali Cations, Halide Anions, and Divalent Cations with Drude Polarizable Models

ion	U_{min}[a]	d_{min}[b]	ΔH[c]	r_{max}	g_{max}	r_{min}	g_{min}	N_c	D[d]	ΔG_{hydr}^{real}[e]	$\Delta\Delta G_{hydr}$[f]
Li$^+$	−35.9 (−35.2)	1.91 (1.87)	−35.6 (−34.0, −34.0)	2.02	12.50	2.56	0.00	4.0	1.30 (1.03)	−120.5	−24.2 (−23.8 to −26.2)
Na$^+$	−24.6 (−24.3)	2.25 (2.26)	−24.4 (−24.0, −25.0)	2.38	7.42	3.24	0.20	5.6	1.58 (1.33)	−96.3	−17.3 (−16.7 to −17.7)
K$^+$	−17.9 (−17.8)	2.62 (2.64)	−17.6 (−17.9, −18.1)	2.74	4.80	3.56	0.45	6.9	2.20 (1.98)	−78.6	−5.2 (−4.9 to −5.4)
Rb$^+$	−15.7 (−16.1)	2.79 (2.79)	−15.2 (−15.9, −16.0)	2.90	4.04	3.80	0.62	8.1	2.44 (2.07)	−73.7	−7.1 (−5.5 to −7.7)
Cs$^+$	−13.3 (−14.1)	3.05 (2.99)	−12.5 (−13.7, −)	3.16	3.25	4.10	0.75	9.7	2.56 (2.06)	−66.5	
F$^-$	−23.5 (−25.9)	2.53 (2.44)	−23.2 (−23.3, −23.3)	2.72	4.77	3.34	0.37	5.5	1.33 (1.48)	−108.0	−30.0 (−13.4 to −30.6)
Cl$^-$	−14.0 (−14.4)	3.09 (3.11)	−13.7 (−13.1, −14.4)	3.16	3.15	3.78	0.72	6.5	1.82 (2.03)	−78.4	−6.5 (−3.3 to −6.9)
Br$^-$	−12.4 (−12.7)	3.26 (3.26)	−11.9 (−12.6, −13.0)	3.28	2.70	3.96	0.75	6.8	1.85 (2.08)	−71.6	−8.5 (−7.7 to −11.1)
I$^-$	−10.2 (−10.6)	3.56 (3.50)	−9.7 (−10.2, −10.5)	3.50	2.28	4.16	0.90	7.1	2.02 (2.05)	−63.1	
Zn^{2+}	−100.0 (−96.3)	1.82 (1.86)	−99.4 (−103.1)	2.14	17.2	3.08	0.0	6.0	0.61 (0.70)	−460.2	−90.3 (−107.6)
Mg^{2+}	−89.4 (−77.9)	1.86 (1.93)	−89.0 (−81.8)	2.06	19.0	2.72	0.0	6.0	0.82 (0.71)	−447.2	−77.3 (−77.7 to −80.3)
Ca^{2+}	−55.6 (−54.9)	2.18 (2.25)	−55.1 (−56.5)	2.28	16.9	2.76	0.0	6.0	0.96 (0.79)	−369.9	−32.7 (−29.8 to −32.9)
Sr^{2+}	−45.2 (−40.6)	2.30 (2.52)	−44.7 (−)	2.42	11.9	3.20	0.0	7.2	0.96 (0.79)	−337.2	−27.2 (−27.9 to −31.1)
Ba^{2+}	−37.7 (−34.0)	2.56 (2.73)	−37.3 (−)	2.68	10.4	3.30	0.1	8.2	0.97 (0.85)	−310.0	

[a] The reference binding energy in parentheses U_{min} of monovalent monohydrates is taken from various sources:[29] Li$^+$,[73] Na$^+$,[74] K$^+$,[75] Rb$^+$,[74] Cs$^+$,[74] F$^-$,[76] Cl$^-$,[76] Br$^-$,[76] I$^-$.[76] The reference values for divalent ions were obtained with MP2 calculations with basis set 6-311++G(3df,3pd) for hydrogen, oxygen, Mg^{2+}, Ca^{2+}, and Zn^{2+} and LANL2DZ pseudopotential and associated basis set for Sr^{2+} and Zn^{2+}. The energies are in kcal/mol. [b] The reference distance in parentheses of the alkali cations is taken from various sources,[29] while those of the halide anions are taken from ref 76. The reference values for divalent cations were obtained from MP2 calculations (see footnote *a* of this table for details). The distances are in Ångstroms. [c] The reference enthalpies in parentheses ΔH for the monovalent monohydrates are taken from the experimental studies.[71,72] The reference enthalpies in parentheses ΔH for the divalent monohydrates are taken from the theoretical study.[87] The enthalpies are in kcal/mol. [d] The experimental self-diffusion coefficients are taken from the *Handbook of Chemistry and Physics*.[95] The self-diffusion coefficients are in 10^{-5} cm^2/s. [e] The *real* hydration free energies ΔG_{hydr}^{real}, in kcal/mol, are obtained from the *intrinsic* free energies from periodic boundary condition (PBC) simulations corrected with the phase potential- and entropy-related contributions. [f] The experimental hydration free energy differences in kcal/mol for the monovalent ions are taken from refs 72 and 78−83, while those for the divalent ions are taken from refs 80, 82, and 83. The entry for Zn^{2+} is defined as ΔG_{hydr}^{real} (Zn^{2+}) − ΔG_{hydr}^{real}(Ca^{2+}).

reported by Mahan,[65] for the alkali cations and a set of "solvent-renormalized" values for the anion halides, with the bare gas-phase polarizability[66] scaled down by a factor of 0.724. Although the actual values vary, such reduced anion polarizabilities have also been noted in previous quantum mechanical studies;[67−70] see ref 29 for a more complete discussion. For the divalent cations, gas-phase values were again taken from Mahan:[65] 0.075 Å^3 for Mg^{2+}, 0.49 Å^3 for Ca^{2+}, 0.87 Å^3 for Sr^{2+}, 1.56 Å^3 for Ba^{2+}, and 0.42 Å^3 for Zn^{2+}.

2.4.2. Ionic Monohydrates. For the monovalent ions, the target monohydrate properties are the same as those used in a previous effort[29] and are summarized in Table 2. Namely, the target binding enthalpies, ΔH, for the alkali cations and halide anions are the gas-phase binding enthalpies measured by Džidić and Kebarle[71] and Tissandier et al.[72] In addition, the binding energies are taken from the ab initio computations.[73−76] A set of target ion−oxygen distances was established for the monovalent ions as described in detail

by Lamoureux and Roux.[29] For the divalent cations, ab initio quantum chemical computations were carried out at the MP2 level using Gaussian03.[77] The details of the basis sets used and resulting target data are presented in Table 2. In these computations, the water geometry was fixed to that of the SWM4-NDP model while the ion−oxygen separation was varied.

2.4.3. Absolute Hydration Free Energies. The experimentally determined absolute hydration free energies of ions at infinite dilution are a central piece of information to optimize the model.[72,78−83] However, as noted previously,[29] there is a large spread in the reported values for the alkali and halide ions (see Figure 2 of ref 29). The same is true for the divalent cations. Considerations based on interfacial potentials may help explain the origin of some of those discrepancies, although it is important to realize that the overall offset of the absolute hydration free energy scale measured experimentally remains undetermined. The most reliable target data that can be extracted from the experimental measurements are the
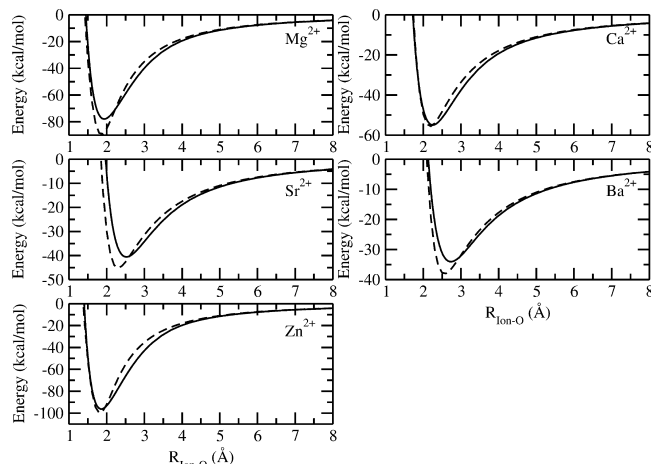
Simulating Monovalent and Divalent Ions

J. Chem. Theory Comput., Vol. 6, No. 3, 2010 **779**

Figure 2. Binding energies of the divalent monohydrates as a function of the distance between the ion and the oxygen atoms: (solid line) ab initio results; (dashed line) Drude. See Table 2 footnotes for the theory and basis set used to obtain the reference data.

relative hydration free energies between different ions of identical charge and the total solvation free energies of neutral salts ($\Delta G_{\text{hydr}}(AB_n) = \Delta G_{\text{hydr}}(A) + n\,\Delta G_{\text{hydr}}(B)$). Notwithstanding those issues, it should be noted there are also some quantitative differences among the various experimental values. For example, Tissandier et al.[72] reported the total hydration free energy of KCl to be -156.8 kcal/mol, while Randles[78] reported -151.3 kcal/mol. The values from Tissandier,[72] Schmid,[83] and Klots[81] are quite close for the monovalent ions. During the parametrization of monovalent ions, we principally aimed to reproduce the target data generated from the measurements of Tissandier.[72] For the divalent ions, the target data was taken from the measurements of Schmid,[83] except in the case of Zn^{2+} where our model falls between the data from Schmid[83] and Gomer and Tryson.[80]

2.4.4. Optimization Procedure. The parameters for the ion−water oxygen interaction are constructed via the Lorentz−Berthelot combination rule,[46] $E_{\text{min}}^{\text{iw}} = (E_{\text{min}}^{\text{ion}} E_{\text{min}}^{\text{O}})^{1/2}$ and $R_{\text{min}}^{\text{iw}} = (R_{\text{min}}^{\text{ion}} + R_{\text{min}}^{\text{O}})/2$. The adjustable parameters for the monatomic ions within the classical Drude oscillator scheme are the LJ parameters of the ion, $R_{\text{min}}^{\text{ion}}$ and $E_{\text{min}}^{\text{ion}}$. Rather than exploring the LJ parameters of the ions directly, it is more convenient to explore the space of monohydrate interaction energies and minimum-energy ion−oxygen distances $\{d_{\text{min}}, U_{\text{min}}\}$,[29] which can be compared to the available ab initio or experimental data. Furthermore, quadratic response functions are fitted to the data from explicit computations, defined by coordinates in $\{d_{\text{min}}, U_{\text{min}}\}$, to interpolate predicted properties (e.g., hydration free energy) between simulated models[29,35]

$$\Delta \bar{G}_{\text{hydr}}(d_{\text{min}}, U_{\text{min}}) = a_0 + a_1 d_{\text{min}} + a_2 U_{\text{min}} + a_3 d_{\text{min}}^2 + \\ a_4 d_{\text{min}} U_{\text{min}} + a_5 U_{\text{min}}^2 \quad (9)$$

A set of polarizable models for the monovalent ions was thus constructed by determining the LJ parameters spanning a grid in the $\{U_{\text{min}}, d_{\text{min}}\}$ coordinates and simultaneously fitting all ions using the interpolated polynomials. For

divalent cations that use the Thole screening as described by eq 7, there are three parameters to fit per ion: the LJ radius and well depth of the ion and the ion−water Thole screening factor. To simplify the parametrization process and ensure physically reasonable dispersive interactions, it proved useful to first assign the LJ well depth by making use of the familiar London dispersion formula $\sim C_6^{ij}/r^6$ for the leading order dispersion coefficient

$$C_6^{\text{iw}} = \frac{3}{2}\left(\frac{E_I^i E_I^w}{E_I^w + E_I^i}\right)\alpha_i \alpha_w \quad (10)$$

where E_I^i, E_I^w, α_i, and α_w are the ionization energy and polarizabilty of the ion and water, respectively. Converting C_6^{iw} into the attractive coefficient of the LJ interaction, $2E_{\text{min}}^{\text{iw}}(R_{\text{min}}^{\text{iw}})^6$, yields an estimate of $E_{\text{min}}^{\text{iw}}$. The resulting values are 0.05 for Mg^{2+}, 0.21 for Ca^{2+}, 0.34 for Sr^{2+}, 0.60 for Ba^{2+}, and 0.25 for Zn^{2+} (all in kcal/mol). Once the LJ well depth is assigned, a grid in $\{d_{\text{min}}, U_{\text{min}}\}$ was generated for each divalent ion by varying the LJ radius and Thole parameter for each ion. The parametrization of the complete set of ion models is fairly consistent and robust. As observed previously,[29,84] alternative sets of parameters can be found with small variations in the ion monohydrate energies (± 0.25 kcal/mol) or in the ion−water distances (± 0.1 Å), resulting in small shifts in the absolute hydration free energies (± 3 kcal/mol). At this stage, the parametrization procedure is aimed at designing accurate models for the infinite dilution limit. Solutions at high concentrations, where ion−ion interactions become important, will be examined in a later stage. The final fitted values are summarized in Table 1.

3. Results and Discussion

The previously developed K^+ model was shown to capture the essential properties in both the gas phase and aqueous solution.[84] The parameters for the polarizable Drude ion models were optimized to be consistent with bulk hydration free energies of the neutral salts while yielding accurate energies and geometries for the ionic monohydrates. An important advantage of reproducing the bulk hydration free energies of neutral salts with our model ions is that these data contain no undetermined offset constant, as do the absolute hydration free energies of individual ions.[29] Achieving an accurate description for the ionic monohydrates becomes critical, therefore, to "lock down" the absolute scale for the bulk hydration free energies. As shown in Table 2, this procedure defines a "solvation-consistent" scale for the absolute hydration free energies of ionic species despite the uncertainties in the experimental data. Overall, the properties of bulk solvation given in Table 3 and small gas-phase clusters given in Table 4 are in excellent agreement with experiments.

3.1. Instabilities and Overpolarization. The polarizable Drude models based on the simple scheme presented by eq 1 yield numerically stable simulations for all the monovalent cations. As expected, based upon substitution into eq 4, no numerical instabilities based on overpolarization were present. In contrast, eq 4 can be used to predict overpolarization catastrophes that occur for halide anions (Br^- and I^-) when

Table 3. Hydration Free Energy of Neutral Salts (in kcal/mol)[a]

	Li+	Na+	K+	Rb+	Cs+
F−	−228.5 (−229.0)	−204.3 (−203.8)	−186.6 (−186.6)	−181.7 (−181.2)	−174.5 (−173.8)
Cl−	−198.9 (−199.3)	−174.7 (−174.0)	−157.0 (−156.8)	−152.1 (−151.4)	−144.9 (−144.0)
Br−	−192.1 (−192.9)	−167.9 (−167.6)	−150.2 (−150.4)	−145.3 (−145.0)	−138.1 (−137.6)
I−	−183.6 (−183.9)	−159.4 (−158.7)	−141.7 (−141.5)	−136.8 (−136.1)	−129.6 (−128.7)

	Zn2+	Mg2+	Ca2+	Sr2+	Ba2+
F−	−676.2 (−696.8)	−663.2	−585.9 (−589.4)	−553.2	−526.0 (−528.1)
Cl−	−617.0 (−637.2)	−604.0 (−607.0)	−526.7 (−529.9)	−494.0 (−499.0)	−466.8 (−468.6)
Br−	−603.4 (−624.4)	−590.4 (−594.3)	−513.1 (−517.0)	−480.4 (−486.2)	−453.2 (−455.7)
I−	−586.4 (−606.5)	−573.4 (−576.4)	−496.1 (−499.1)	−463.4 (−468.3)	−436.2 (−437.8)

[a] The experimental solvation free energies reported for alkali halide salts by Tissandier et al.[72] and Klots[81] (Cs+) are listed in parentheses for comparison. The experimental solvation free energies for salts of divalent cations were derived from the free energies of formation of the salt minus that of the gas-phase ions (in kJ/mol): $\Delta G^\circ_{aq}(A^{n+} + nB^-) = \Delta G^\circ_f(AB_n) - \Delta G^\circ_f(A^{n+}(g)) - n\Delta G^\circ_f(B^-(g))$, with $\Delta G^\circ_f(A^{n+}(g)) = \Delta H^\circ_f(A^{n+}(g)) - T\Delta S^\circ_f(A^{n+}(g))$ and $\Delta S^\circ_f(A^{n+}(g)) = 108.8555 + 12.4716 \ln(M) - v^* S(A^*) \pm nS(e^-(g))$, where M is the molar mass in grams, v^* is 1/2 for anions and 1 for cations, $S(A^*)$ is the element's absolute entropy in the standard state, and $S(e^-(g))$ is the absolute entropy of the gaseous electron (see ref 72 for details). The experimental thermodynamic data are taken from the *Handbook of Chemistry and Physics*[95] and the 1982 NBS tables.[85]

Table 4. Solvation Enthalpies of Ion M in Water Clusters $(H_2O)_n$ (in kcal/mol)

ions, M	model/exp	solvation enthalpy					
		1	2	3	4	5	6
Li+	Drude	−35.6	−65.3 (−29.7)	−87.0 (−21.7)	−103.0 (−16.0)	−114.2 (−11.2)	−125.3 (−11.1)
	exp[72]	−34.0	−59.8 (−25.8)	−80.5 (−20.7)	−96.9 (−16.4)	−110.8 (−13.9)	−122.9 (−12.1)
	exp[71]	−34.0	−59.8 (−25.8)	−80.5 (−20.7)	−96.9 (−16.4)	−110.8 (−13.9)	−122.9 (−12.1)
Na+	Drude	−24.4	−45.9 (−21.5)	−63.4 (−17.5)	−77.2 (−13.8)	−87.0 (−9.8)	−95.1 (−8.1)
	exp[72]	−25.0	−44.8 (−19.8)	−60.2 (−15.4)	−73.4 (−13.2)	−84.9 (−11.5)	−95.6 (−10.7)
	exp[71]	−24.0	−43.8 (−19.8)	−59.6 (−15.8)	−73.4 (−13.8)	−85.7 (−12.3)	−96.4 (−10.7)
K+	Drude	−17.6	−33.2 (−15.6)	−47.0 (−13.8)	−58.6 (−11.6)	−67.7 (−9.1)	−76.0 (−8.3)
	exp[72]	−18.1	−34.2 (−16.1)	−47.4 (−13.2)	−59.2 (−11.8)	−69.9 (−10.7)	−79.9 (−10.0)
	exp[71]	−17.9	−34.0 (−16.1)	−47.2 (−13.2)	−59.0 (−11.8)	−69.7 (−10.7)	−79.7 (−10.0)
Rb+	Drude	−15.3	−29.0 (−13.7)	−41.2 (−12.2)	−51.9 (−10.7)	−60.3 (−8.4)	−68.5 (−8.2)
	exp[72]	−16.0	−29.6 (−13.6)	−41.8 (−12.2)	−53.0 (−11.2)	−63.5 (−10.5)	
	exp[71]	−15.9	−29.5 (−13.6)	−41.7 (−12.2)	−52.9 (−11.2)	−63.4 (−10.5)	
Cs+	Drude	−12.4	−24.3 (−11.9)	−34.7 (−10.3)	−44.0 (−9.3)	−52.0 (−8.0)	−64.0 (−12.0)
	exp[71]	−13.7	−26.2 (−12.5)	−37.4 (−11.2)	−48.0 (−10.6)		
F−	Drude	−23.2	−45.4 (−22.2)	−66.9 (−21.5)	−80.2 (−13.3)	−90.7 (−10.5)	−103.1 (−12.4)
	exp[72]	−23.3	−41.2 (−17.9)	−55.7 (−14.5)	−69.4 (−13.7)	−82.2 (−12.8)	−93.1 (−10.9)
Cl−	Drude	−13.7	−27.6 (−13.9)	−43.9 (−16.3)	−57.4 (−13.5)	−64.4 (−7.0)	−71.7 (−7.3)
	exp[72]	−14.4	−27.2 (−12.8)	−38.9 (−11.7)	−49.8 (−10.9)	−59.3 (−9.5)	−68.1 (−8.8)
Br−	Drude	−11.9	−24.6 (−12.7)	−40.4 (−15.8)	−53.2 (−12.8)	−59.6 (−6.4)	−68.1 (−8.5)
	exp[72]	−13.0	−25.0 (−12.0)	−36.4 (−11.4)	−47.4 (−11.0)	−58.2 (−10.8)	−68.5 (−10.3)
I−	Drude	−9.7	−20.9 (−11.2)	−35.6 (−14.7)	−42.4 (−6.8)	−50.7 (−8.4)	−59.6 (−8.9)
	exp[72]	−10.5	−20.2 (−9.7)	−29.5 (−9.3)	−38.7 (−9.2)	−47.7 (−9.0)	
Zn2+	Drude	−99.4	−176.9 (−77.5)	−237.2 (−60.3)	−284.4 (−47.2)	−306.2 (−21.8)	−329.0 (−22.8)
	theor or exp[87]	−103.1	−191.1 (−88.0)	−246.9 (−55.8)	−289.8 (−42.9)	−314.8 (−25.0)	−339.0 (−24.2)
Mg2+	Drude	−89.0	−164.6 (−75.6)	−223.3 (−58.7)	−269.8 (−46.5)	−293.0 (−23.2)	−316.5 (−23.5)
	theor or exp[87]	−81.8	−153.8 (−72.0)	−210.4 (−56.6)	−254.3 (−43.9)	−282.3 (−28.0)	−306.9 (−24.6)
Ca2+	Drude	−55.1	−105.2 (−50.1)	−149.5 (−44.2)	−188.1 (−38.6)	−217.8 (−29.7)	−245.3 (−27.5)
	theor or exp[87]	−56.5	−105.1 (−48.5)	−148.0 (−42.9)	−183.6 (−35.6)	−211.3 (−27.7)	−236.6 (−25.3)
Sr2+	Drude	−44.7	−86.2 (−41.5)	−124.0 (−37.8)	−158.4 (−34.4)	−187.0 (−28.6)	−213.6 (−26.6)
	exp[86]						− (−22.7)
Ba2+	Drude	−37.3	−72.0 (−34.7)	−103.7 (−31.7)	−133.3 (−29.6)	−158.7 (−25.4)	−182.6 (−23.9)
	exp[86]					− (−23.9)	− (−19.8)

[a] Numbers in parentheses are for the reaction $M(H_2O)_{n-1} + H_2O \rightleftharpoons M(H_2O)_n$.

ion−proton separations are within physically realistic distances. Such instabilities are not present in our previously published set of alkali−halide ionic models[29] because the positive Drude particle and proton do not attract one another. Introducing an anharmonic restoring force to the anionic Drude oscillator removes those instabilities by preventing excessively large excursions of the Drude particle away from the ion. Importantly, as shown in Tables 2−4, this construction did not affect our ability to adjust the parameters of the model to accurately fit the target data. In particular, the

properties of the small cluster hydrates can be reproduced with the simple anharmonic restoring spring.

A more serious overpolarization problem is encountered with the divalent cations. We first tried the two simple schemes to solve this issue, namely, adding an anharmonic restoring force to the Drude oscillator or adding a LJ core repulsion between the oxygen-tethered Drude particle and the divalent cations. Experimenting with various parametrizations showed that while introducing an anharmonic restoring force or a LJ core can prevent the numerical
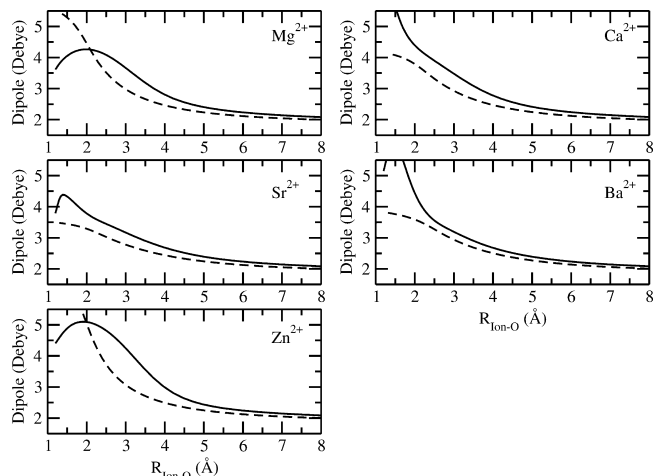
Simulating Monovalent and Divalent Ions

J. Chem. Theory Comput., Vol. 6, No. 3, 2010 **781**

Figure 3. Total dipole moments of the divalent monohydrates as a function of the distance between the ion and the oxygen atoms. The ions are located at the origin to compute the dipole moment. See Table 2 for details.

instabilities, it remained difficult to get reasonable monohydrate energies as the large Coulombic repulsion between the bare positive charge carried by the oxygen nucleus and the ion remains unshielded. This Coulombic interaction gives rise to large repulsion energies that must be compensated in order to have reasonable monohydrate energies and geometries with the divalent cations. Ultimately, it was found that introducing a Thole-type screening function[49] for the Coulombic electrostatic for the interactions between the divalent ion and the induced dipole component of the water molecules led to the best models. A similar approach was used to construct models of divalent ions consistent with the AMOEBA polarizable force field.[30,52] Comparisons between the Drude model with Thole-like damping and the ab initio calculations are shown in Figures 2 and 3. The Thole screening scheme given by eq 7 effectively removes the singularity problems illustrated in Figure 1 and yields divalent monohydrates with reasonable binding energies and total dipole moments.

3.2. Bulk Hydration Free Energies. The total hydration free energies of neutral salts are shown in Table 3 and Figures 4 and 5 together with available experimental data. Although the relative hydration free energy difference between different ions in the same series and the total hydration free energy of a neutral salt can generally be measured very accurately, we note that there are noticeable differences among the experimental data from difference sources[72,78−83,85] (see Supporting Information Tables S1 and S2). Overall, the current Drude models agree very well with the experimental data, with the monovalent neutral salts closer to the experimental estimations by Tissandier et al.,[72] Klots,[81] and Schmid et al.[83] (Figure 4) and the divalent neutral salts closer to the experimental estimations by Schmid et al.[83] and Gomer and Tryson[80] (Figure 5).

The hydration free energy differences of ions in the same series are well reproduced with some compromise of the monohydrate properties for smaller ions. These present models define an absolute hydration free energy scale in which the *real* hydration free energy of the proton would be
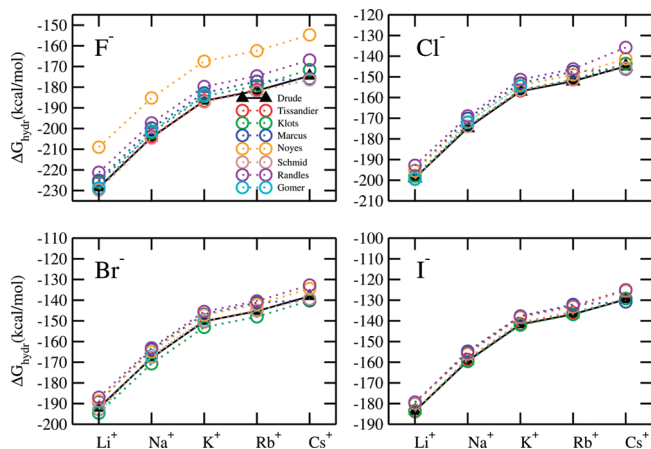

Figure 4. Hydration free energies of salts with monovalent cations: Tissandier,[72] Klots,[81] Marcus,[82] Noyes,[79] Schmid,[83] Randles,[78] and Gomer.[80]
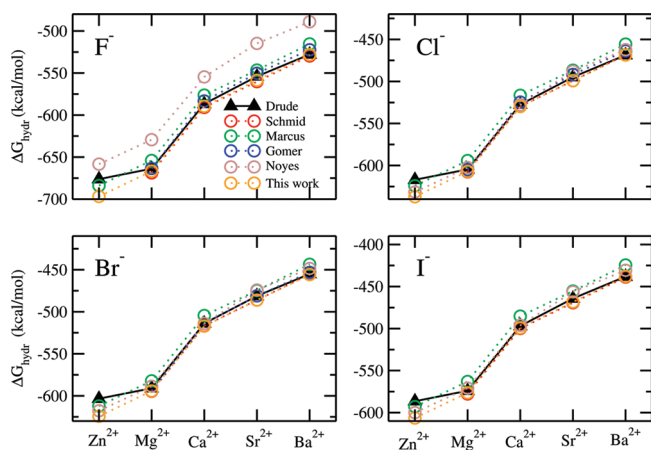

Figure 5. Hydration free energies of salts with divalent cations: Schmid,[83] Marcus,[82] Gomer,[80] Noyes,[79] and this work. See the caption of Table 3 for details. The entries for MgF_2 and SrF_2 in this work were derived based on hydration free energy differences between F^- and Cl^- and the total hydration free energies of salts $MgCl_2$ and $SrCl_2$.

−258.8 kcal/mol. This can be compared with the experimental estimates of −264 kcal/mol by Tissandier et al.,[72] −249.5 kcal/mol by Schmid et al.,[83] and −253.2 kcal/mol by Gomer and Tryson.[80] It is noteworthy that the current value of −258.8 kcal/mol differs by less than 2% from the experimental estimates obtained by Tissandier et al.[72] This suggests that their analysis, which consisted of monitoring the stepwise changes in ion−cluster free energies, was targeting the absolute *real* free energy of the proton.[72]

3.3. Enthalpies of Ionic Small Hydrates. Structural and thermodynamic properties of small clusters offer a rigorous test of the accuracy of the models. As opposed to bulk liquid hydration where induced polarization over different moieties may lead to some compensation of errors, the microscopic interactions are displayed nakedly in small clusters, and possible limitations of the models become readily apparent. Furthermore, because the polarizable models are constructed with the intended purpose of responding accurately to different electrostatic environments, the ability to reproduce the properties of small ionic hydrates is very important. Finally, the properties of the ionic monohydrates are used
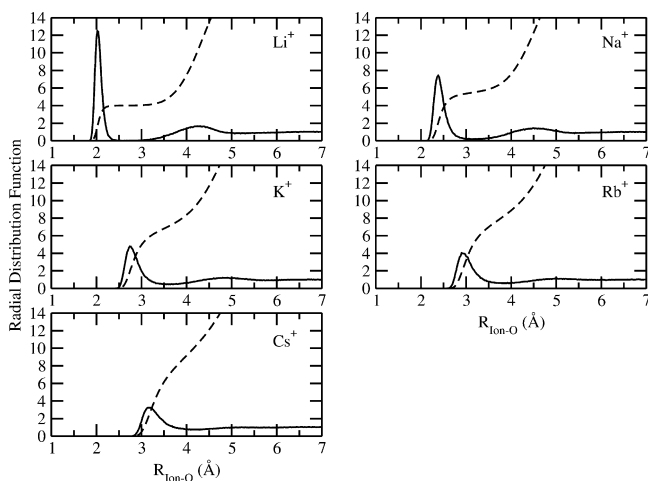
Figure 6. Radial hydration structure for the alkali cations. Radial distribution functions $g(R_{\text{Ion}-\text{O}})$ functions are shown by the solid line, and the coordination numbers $N(R_{\text{Ion}-\text{O}})$ are shown by the dashed line.

to set the scale for the absolute hydration free energies in bulk solution. The calculated ionic monohydrate energies and geometries are reported in Table 2. The results generally agree well with the target data.[73−76] As previously noted,[29] the limitations of the models are most apparent for smaller ions. This trend is observed for the divalent cations as well. The less satisfactory performance of the divalent cations is very likely due to the neglect of the important charge-transfer effect, which is absent from the current energy function. The enthalpies of hydration for an ion solvated in a small water cluster (1−6) compare favorably with literature values with the monovalent cations having the best agreement[71,72,86,87] (Table 4). In general, the monovalent cations reproduce the experimentally measured properties of ionic hydrate clusters slightly better than do the halide anions. The most likely explanation for this is that the conformational spaces for water molecules in the anion−water clusters are far more complicated than those for the cation−water clusters due to the formation of hydrogen bonding between water molecules coordinating the anion. The hydration enthalpies for the divalent cations have larger deviation from the experimental or ab initio data, consistent with the monohydrate properties.

3.4. Coordination Structure in Bulk Solution. Radial distribution functions (RDF) averaged from 10 simulations each of 200 ps for ion−oxygen contacts, $g(R_{\text{Ion}-\text{O}})$, are presented in Figures 6, 7, and 8 for the alkali cations, halide anions, and divalent ions, respectively. The coordination numbers for each ion, $N(R_{\text{Ion}-\text{O}})$, defined as the integral of $g(R_{\text{Ion}-\text{O}})$ from the origin out to the first minimum, r_{min}, are presented in Table 2. The RDFs and coordination numbers for the monovalent ions are very similar to those reported from the previous models (Figures 6 and 7) based upon the (positive Drude) SWM4-DP water model.[29] Here, we briefly discuss the main findings.

In accordance with the most recent computational studies, the current model predicts that the Li$^+$ ion is 4-coordinated within the experimental range obtained from neutron and X-ray diffraction (see refs 88−90 for a survey). After the first peak, the lithium−oxygen RDF remains very small over a large interval extending from 2.4 to 3.1 Å. This result is
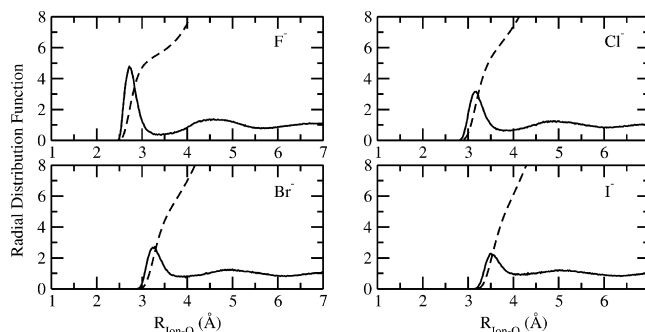

Figure 7. Radial hydration structure for the halide anions. Radial distribution functions $g(R_{\text{Ion}-\text{O}})$ are shown by the solid line, and the coordination numbers $N(R_{\text{Ion}-\text{O}})$ are shown by the dashed line.
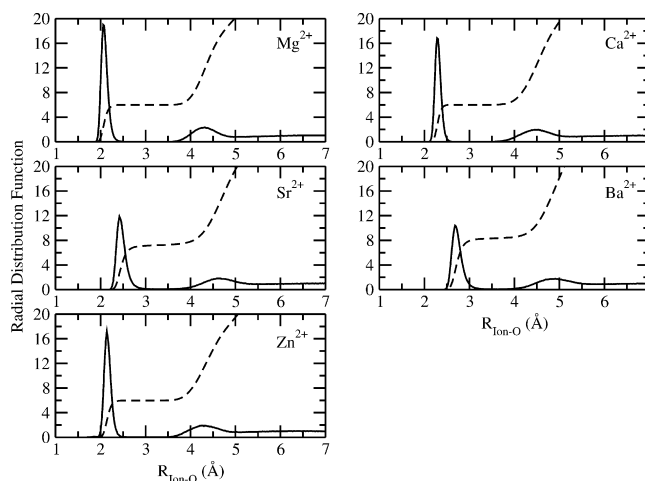

Figure 8. Radial hydration structure for the divalent cations. Radial distribution functions $g(R_{\text{Ion}-\text{O}})$ functions are shown by the solid line, and the coordination numbers $N(R_{\text{Ion}-\text{O}})$ are shown by the dashed line.

consistent with Car−Parrinello molecular dynamics (CPMD) simulation.[91] The strong separation between the first and second peak in the RDF implies that the coordination number of Li$^+$ can be defined unambiguously. However, for Na$^+$ and K$^+$, a more populated region is observed between the first and second peaks in the RDFs. As a result, a broad distribution of coordination numbers within the first solvation shell was observed.[22,84] As dissussed in refs 29, 84, and 90, both experimental studies and CPMD-type simulations have predicted a wide range of coordination numbers for Na$^+$ and K$^+$ and the current models fall well within the reported range. In addition, the coordination number distributions of Na$^+$ and K$^+$ overlap substantially with one another, indicating that the coordination number alone is not a dominant factor in describing the thermodynamics of ion solvation.[22]

For the divalent ions, the first peak in the RDF is generally sharper than those of the monovalent ions, indicating a highly ordered water structure around the ions (Figure 8). In addition, a clear separation exists between the first and the second coordination shells, as indicated by the small value of the first minimum in the RDFs. The current Drude model for Ca^{2+} gives a coordination number of 6, smaller than the value of 7.3 based on the AMOEBA force field.[30] As a comparison, the coordination numbers of Ca^{2+} were esti-

Simulating Monovalent and Divalent Ions

J. Chem. Theory Comput., Vol. 6, No. 3, 2010 **783**

Table 5. Effective Self-Diffusion Coefficients[a] of the Neutral Salts in 10^{-5} cm²/s (the experimentally derived values are in parentheses)[95]

	Li⁺	Na⁺	K⁺	Rb⁺	Cs⁺
F⁻	1.32 (1.25)	1.45 (1.40)	1.77 (1.73)	1.89 (1.78)	1.95 (1.77)
Cl⁻	1.56 (1.53)	1.70 (1.68)	2.01 (2.01)	2.13 (2.05)	2.19 (2.05)
Br⁻	1.58 (1.56)	1.72 (1.71)	2.02 (2.03)	2.15 (2.08)	2.21 (2.07)
I⁻	1.66 (1.54)	1.80 (1.69)	2.11 (2.01)	2.23 (2.06)	2.29 (2.06)

	Zn²⁺	Mg²⁺	Ca²⁺	Sr²⁺	Ba²⁺
F⁻	0.85 (0.96)	0.99 (0.97)	1.08 (1.02)	1.08 (1.02)	1.09 (1.06)
Cl⁻	1.01 (1.14)	1.15 (1.15)	1.25 (1.20)	1.25 (1.20)	1.25 (1.25)
Br⁻	1.02 (1.16)	1.16 (1.17)	1.26 (1.22)	1.26 (1.22)	1.26 (1.26)
I⁻	1.08 (1.15)	1.22 (1.16)	1.31 (1.21)	1.31 (1.21)	1.32 (1.25)

[a] The effective self-diffusion coefficients for the neutral salts are defined as $D_{eff} = \sum_i z_i^2 D_i / \sum_i z_i^2$.

mated to lie between 5.5 and 10 based on various experimental techniques[92] and between 6 and 7 according to the most recent CPMD simulations.[92] For Mg²⁺, the Drude model gives a coordination number of exactly 6, consistent with both the experimental[93] and the ab initio[94] studies. For Zn²⁺, the coordination number is estimated to be 6, which is within the experimentally estimated range from 5.3 to 6.6.[88] Overall, the coordination structure for the ion models is in excellent agreement with experiment, given that no direct adjustments were made to reproduce those features during the parametrization.

3.5. Self-Diffusion Coefficients. The ability of the polarizable force field to reproduce the dynamic transport properties of ions in aqueous solutions is a critical test of the accuracy of computational models. This ability is best characterized by considering the diffusion of ions in aqueous solutions. The self-diffusion coefficients for the ion models at infinite dilution were computed from the mean-square displacement correlation function. Because there is only a single ion in the atomic system, relatively long simulations are required to obtain converged self-diffusion coefficients. To improve convergence, 10 simulations of 200 ps each were averaged for each ion. The results are presented in Tables 2 and 5. Additional simulations indicate that the current estimates from MD are not overly sensitive to finite-size effects within PBC.

The agreement between the Drude model and the available experimental values[95] is relatively good. Interestingly, the calculated values appear to be slightly overestimated for the cations while they are underestimated for the anions. This intriguing trend, with the cations diffusing faster and the anions slower than the experimental estimates, has also been noted in a recent study with nonpolarizable models.[17] Limitations in the ions and/or solvent models could perhaps explain these discrepancies. However, it is worth recalling that the polarizable SWM4-NPD water model matches the experimental value of the self-diffusion of water exactly, and the shear viscosity is satisfactorily reproduced as well.[35] Alternatively, there is also the possibility that the experimental estimates for the single ions are at fault for the following reason. Experimentally, it is nearly impossible to measure the self-diffusion coefficient of isolated ions in solution. Most of the available values for individual cations

and anions have been deduced from conductivity measurements of electrolyte aqueous solutions by invoking additional hypotheses.[95] In the limit of very low concentration [c], the conductivity σ of an electrolyte solution varies as $[c](e^2/k_BT)\sum_i z_i^2 D_i$. In practice, all the ionic species of a neutral salt contribute to the experimentally observed σ, suggesting that a more meaningful comparison is achieved by considering the effective self-diffusion coefficients for neutral salts, $D_{eff} = \sum_i z_i^2 D_i / \sum_i z_i^2$, corresponding to the low concentration limit of the whole salt conductivity after removing the dependence on the trivial prefactor $[c](e^2/k_BT)\sum_i z_i^2$.

In Table 5 the calculated and experimental values of D_{eff} for 40 neutral salts are listed. The agreement between the experimental data and the calculations is striking. With the exclusion of salts involving the smallest anion, F⁻, the calculated values for the alkali−halides are almost perfect, while the salts with the divalent cations are all less than a few percent off. The remarkable agreement shown in Table 5 strongly argues in favor of the importance of considering the experimental transport properties of neutral salts rather than reported values for the self-diffusion coefficients of individual ions.

3.6. Comparison with Other Models. Over the years, a number of nonpolarizable[13−18,96] and polarizable[28−30,84] models of the monovalent ion series have been developed and parametrized to reproduce different sets of target data. Previous nonpolarizable models have been parametrized primarily on the basis of the absolute hydration free energies of single ions.[13−15,18,96] Recently, Joung and Cheatham pushed the limit of nonpolarizable force fields by enforcing a balanced description of crystal and solution properties.[16,17] Induced polarization is not a dominant factor for the hydration of a large cation like K⁺, and satisfactory results can be obtained with nonpolarizable models.[84] Nevertheless, adopting nonpolarizable models often leads to some compromises concerning the gas-phase properties (e.g., the monohydrate properties)[15] or the dynamic propeties (e.g., the self-diffusion constant).[17] Furthermore, the nonpolarizable models are calibrated for bulk solutions, and their validity in different environments is uncertain. In contrast, the polarizable force fields improve the transferability by capturing the electronic polarization in different environments.[28−30,84] The AMOEBA models, an extension of the induced dipole model, developed by Ponder and co-workers,[28,30] accurately reproduce the various gas-phase and condensed-phase properties of ions, with more complex terms for electrostatics. One important difference of the polarizable models developed here compared to AMOEBA, where multipolar electrostatic terms are required, is that all the interactions are charge−charge Coulombic interactions and the functional form of the potential energy terms can be implemented in standard MD codes without major changes.

Another important difference concerns the parametrization strategy. Here, the parametrization sought to reproduce the well-established experimental data (i.e., the total hydration free energy of neutral salts as well as the relative free energy difference between different ions in the same series). By virtue of this procedure, the monohydrate properties served to lock down the absolute free energy scale. The parametri-

zation of the ion models in AMOEBA followed a somewhat similar route, focusing mainly on the monohydrate properties and the neutral salts.[28,30] This is in contrast with other efforts aimed at fitting the actual single-ion hydration free energies presented by a given experimental scale.[13−18,96] As noted previously,[29] we consider this to be problematic because the absolute hydration free energies measured experimentally depend on an undetermined phase potential, which is reflected in the large spread in the reported values. Coincidentally, the final models presented here happen to be close to the single-ion hydration free energies presented by Noyes for the monovalent cations,[79] although this scale was not imposed during parametrization. However, the results from the final models differ markedly from the single-ion hydration free energies presented by several of the experimental scales, and if those values were imposed as target data, then the unavoidable consequence would be a deterioration of the monohydrate properties. These considerations highlight the pitfalls with using the absolute single-ion hydration free energy reported from experiments as target data for force field parametrization.

4. Conclusion

In the current study, parameters for both cations and anions (Table 1) were developed for the polarizable force field based on classical Drude oscillator in conjunction with the SWM4-NDP water model. The parameters for the ions have been derived based on the gas-phase monohydrate properties and the hydration free energies in the bulk phase. The various gas-phase and condensed-phase properties (Tables 2−4) are in reasonable agreement with the available experimental data and ab initio calculations. The dynamic transport properties of the models are in excellent agreement with experimental estimates based on electrolyte conductivity (Table 5). Overall, the set of models developed here should provide an important tool for accurate studies of a wide range of biological and physical processes involving ions in aqueous solutions.

The models for divalent cations from the present work are somewhat less accurate than those of the monovalent ions. The results from ab initio quantum chemistry calculations and the hydration free energy are not perfectly reproduced. This could be in part due to the neglect of charge-transfer effects and to the breakdown of linear response.[97] As shown previously, the deviations from linear polarization response become quite severe with a perturbation by a charge of $+2.0e$.[97] In this case, it was necessary to treat the overpolarization that occurs when the ion is in direct contact with a water molecule. Analysis of the functional form of the potential function showed that an overpolarization catastrophe is unavoidable when the distance between a polarizable water and the divalent cation is less than 1.97 Å. By contrast, monovalent cations require no special treatment. Several strategies to avoid overpolarization for the divalent ions were considered. The best approach turned out to be introduction of a Thole-like screening function to modulate the Coulomb electrostatic interactions between the cation and the water molecule. Careful parametrization of this functional form against the results from quantum mechanical calculations led to reasonably accurate models.

A similar approach was used to model Mg^{2+} and Ca^{2+} in the context of the AMOEBA polarizable force field.[30,52]

The present effort at parametrizing a complete set of ion models underlies the difficulties that arise when considering single-ion bulk properties deduced from experiments as objective target data. Experimental measurement of ions in bulk liquid phases are performed on globally neutral systems, and deriving single-ion properties requires additional nonthermodynamic hypotheses. The most meaningful comparisons are made with data directly obtained from neutral salts. For example, while the models do not match the single-ion diffusion coefficients deduced from electrolyte conductivity measurements, the effective diffusion coefficients for the neutral salts are in remarkably good agreement with experiments (Table 5). Such issues become particularly accute with respect to single-ion hydration free energies. Experimental estimates often rely on the free energy associated with the solvation of H^+ as a reference. However, published experimental scales for the alkali−halides solvation free energy can shift up and down, depending upon the chosen reference. Some of the experimental values may appear to be inconsistent with one another, which increases the difficulties in developing an accurate force field. These problems are further compounded by the fact that absolute free energies of charged species are affected by the air−liquid interfacial potential. While the solvation free energies of neutral salts reported in experimental tables are unambiguous and independent of the interfacial potential, absolute hydration free energies of ions are somewhat ambiguous and cannot be readily utilized as the target data for parametrization. Preserving complete consistency of the solvation free energies of all ions has been a critical aspect of the present effort. To extract a reliable set of target data for the absolute hydration free energy as required to parametrize our models, we previously adopted a strategy based on a "solvation-consistent" scale.[29] The consequences of this scale are well illustrated by considering the K^+ model. The parameters of K^+ have been adjusted to fit the properties of small cluster hydrates in the gas phase (Table 4). Once used in bulk-phase simulations, this model yields a (real) hydration free energy of -78.6 kcal/mol (Table 2). Further validating the K^+ model was the level of agreement of K^+−water oxygen radial distributions for the Drude model with results from both experimental and ab initio Born−Oppenheimer and Car−Parrinello MD simulations.[84] Therefore, the absolute free energy scale has been "locked down" by using the K^+ model, which then serves as a central reference for other ionic solutes. This suggests that the parametrization of additional charged moieties should be developed to be in accord with the present solvation-consistent scale.

Finally, it is worth pointing out that at this stage the models have been optimized to be accurate in the infinite dilution limit. The problem associated with electrolyte solutions at high concentrations, where issues of solubility and ion−ion interactions are important, will be examined in the near future. In particular, the models will be tested by calculating

Simulating Monovalent and Divalent Ions

J. Chem. Theory Comput., Vol. 6, No. 3, 2010 **785**

the osmotic pressure of concentrated salt solutions using a new method.[98]

Supporting Information Available: Comparison of the induced dipole moments of Cl^- and Br^- as a function of external electrostatic field strength, and compilation of the experimentally derived hydration free energy differences between different ions. This material is available free of charge via the Internet at http://pubs.acs.org.

References

(1) Hille, B. *Ion channels of excitable membranes*, 3rd ed.; Sinauer Associates: Sunderland, MA, 2001.

(2) Page, M. J.; Di Cera, E. *Physiol. Rev.* **2006**, *86*, 1049–1092.

(3) Dudev, T.; Lim, C. *Chem. Rev.* **2003**, *103*, 773–787.

(4) Torrance, J. W.; MacArthur, M. W.; Thornton, J. M. *Proteins Struct. Funct. Bioinformatics* **2008**, *71*, 813–830.

(5) Schumacher, M.; Rivard, A.; Bachinger, H.; Adelman, J. *Nature* **2001**, *410*, 1120–1124.

(6) Sakharov, D.; Lim, C. *J. Am. Chem. Soc.* **2005**, *127*, 4921–4929.

(7) Bloomfield, V. *Biopolymers* **1991**, *31*, 1471–1481.

(8) Cate, J.; Gooding, A.; Podell, E.; Zhou, K.; Golden, B.; Kundrot, C.; Cech, T.; Doudna, J. *Science* **1996**, *273*, 1678–1685.

(9) Fang, X.; Pan, T.; Sosnick, T. *Nat. Struct. Biol.* **1999**, *6*, 1091–1095.

(10) Draper, D.; Grilley, D.; Soto, A. *Annu. Rev. Biophys. Biomol. Struct.* **2005**, *34*, 221–243.

(11) Woodson, S. *Curr. Opin. Chem. Biol.* **2005**, *9*, 104–109.

(12) Qu, X.; Smith, G. J.; Lee, K. T.; Sosnick, T. R.; Pan, T.; Scherer, N. F. *Proc. Natl. Acad. Sci. U.S.A.* **2008**, *105*, 6602–6607.

(13) Åqvist, J. *J. Phys. Chem.* **1990**, *94*, 8021–8024.

(14) Beglov, D.; Roux, B. *J. Chem. Phys.* **1994**, *100*, 9050–9063.

(15) Jensen, K. P.; Jorgensen, W. L. *J. Chem. Theory Comput.* **2006**, *2*, 1499–1509.

(16) Joung, I. S.; Cheatham, T. E. *J. Phys. Chem. B* **2008**, *112*, 9020–9041.

(17) Joung, I. S.; Cheatham, T. E. *J. Phys. Chem. B* **2009**, *113*, 13279–13290.

(18) Carlsson, J.; Aqvist, J. *J. Phys. Chem. B* **2009**, *113*, 10255–10260.

(19) Roux, B. *Chem. Phys. Lett.* **1993**, *212*, 231–240.

(20) Allen, T. W.; Andersen, O. S.; Roux, B. *Biophys. J.* **2006**, *90*, 3447–3468.

(21) Bucher, D.; Guidoni, L.; Maurer, P.; Rothlisberger, U. *J. Chem. Theory Comput.* **2009**, *5*, 2173–2179.

(22) Yu, H. B.; Roux, B. *Biophys. J.* **2009**, *97*, L15–L17.

(23) Rick, S. W.; Stuart, S. J. *Rev. Comput. Chem.* **2002**, 89–146.

(24) Yu, H. B.; van Gunsteren, W. F. *Comput. Phys. Commun.* **2005**, *172*, 69–85.

(25) Warshel, A.; Kato, M.; Pisliakov, A. V. *J. Chem. Theory Comput.* **2007**, *3*, 2034–2045.

(26) Lopes, P. E. M.; Roux, B.; MacKerell, A. D., Jr. *Theor. Chem. Acc.* **2009**, *124*, 11–28.

(27) Dang, L. X.; Rice, J. E.; Caldwell, J.; Kollman, P. A. *J. Am. Chem. Soc.* **1991**, *113*, 2481–2486.

(28) Grossfield, A.; Ren, P.; Ponder, J. W. *J. Am. Chem. Soc.* **2003**, *125*, 15671–15682.

(29) Lamoureux, G.; Roux, B. *J. Phys. Chem. B* **2006**, *110*, 3308–3322.

(30) Jiao, D.; King, C.; Grossfield, A.; Darden, T.; Ren, P. *J. Phys. Chem. B* **2006**, *110*, 18553–18559.

(31) Drude, P. *Lehrbuch der Optik*; S. Hirzel: Leipzig, 1900.

(32) Sangster, M. J. L.; Dixon, M. *Adv. Phys.* **1976**, *25*, 247–342.

(33) Lamoureux, G.; Roux, B. *J. Chem. Phys.* **2003**, *119*, 3025–3039.

(34) Lamoureux, G.; MacKerell, A. D., Jr.; Roux, B. *J. Chem. Phys.* **2003**, *119*, 5185–5197.

(35) Lamoureux, G.; Harder, E.; Vorobyov, I. V.; Roux, B.; MacKerell, A. D., Jr. *Chem. Phys. Lett.* **2006**, *418*, 245–249.

(36) Dick, B. G., Jr.; Overhauser, A. W. *Phys. Rev.* **1958**, *112*, 90.

(37) Cochran, W. *Crit. Rev. Solid State Mater. Sci.* **1971**, *2*, 1–44.

(38) van Maaren, P. J.; van der Spoel, D. *J. Phys. Chem. B* **2001**, *105*, 2618–2626.

(39) Kunz, A. P.; van Gunsteren, W. F. *J Phys Chem A* **2009**, *113*, 11570–11579.

(40) Vorobyov, I.; Anisimov, V. M.; Greene, S.; Venable, R. M.; Moser, A.; Pastor, R. W.; MacKerell, A. D., Jr. *J. Chem. Theor. Comput.* **2007**, *3*, 1120–1133.

(41) Lopes, P. E. M.; Lamoureux, G.; Roux, B.; MacKerell, A. D., Jr. *J. Phys. Chem. B* **2007**, *111*, 2873–2885.

(42) Anisimov, V. M.; Vorobyov, I. V.; Roux, B.; MacKerell, A. D., Jr. *J. Chem. Theor. Comput.* **2007**, *3*, 1927–1946.

(43) Harder, E.; Anisimov, V. M.; Whitfield, T. W.; MacKerell, A. D., Jr.; Roux, B. *J. Phys. Chem. B* **2008**, *112*, 3509–3521.

(44) Lopes, P. E. M.; Lamoureux, G.; Mackerell, A. D., Jr. *J. Comput. Chem.* **2009**, *30*, 1821–1838.

(45) Harder, E.; MacKerell, A. D., Jr.; Roux, B. *J. Am. Chem. Soc.* **2009**, *131*, 2760–2761.

(46) Allen, M. P.; Tildesley, D. J. *Computer Simulation of Liquids*; Oxford University Press: Oxford, 1987.

(47) Tuckerman, M.; Berne, B. J.; Martyna, G. J. *J. Chem. Phys.* **1992**, *97*, 1990–2001.

(48) Brooks, B. R.; Bruccoleri, R. E.; Olafson, B. D.; States, D. J.; Swaminathan, S.; Karplus, M. *J. Comput. Chem.* **1983**, *4*, 187–217.

(49) Thole, B. T. *Chem. Phys.* **1981**, *59*, 341–350.

(50) van der Hoef, M. A.; Madden, P. A. *Mol. Phys.* **1998**, *94*, 417–433.

(51) Whitfield, T. W.; Martyna, G. J. *Chem. Phys. Lett.* **2006**, *424*, 409–413.

(52) Piquemal, J. P.; Perera, L.; Cisneros, G. A.; Ren, P.; Pedersen, L. G.; Darden, T. A. *J. Chem. Phys.* **2006**, *125*, 054511.

(53) Deng, Y.; Roux, B. *J. Phys. Chem. B* **2004**, *108*, 16567–16576.

(54) Essmann, U.; Perera, L.; Berkowitz, M. L.; Darden, T.; Lee, H.; Pedersen, L. G. *J. Chem. Phys.* **1995**, *103*, 8577–8593.

(55) Nosé, S. *J. Chem. Phys.* **1984**, *81*, 511–519.

(56) Hoover, W. *Phys. Rev. A* **1985**, *31*, 1695–1697.

(57) Martyna, G.; Tobias, D.; Klein, M. *J. Chem. Phys.* **1994**, *101*, 4177–4189.

(58) Ryckaert, J. P.; Ciccotti, G.; Berendsen, H. J. C. *J. Comput. Phys.* **1977**, *23*, 327–341.

(59) Martyna, G. J.; Tuckerman, M. E.; Tobias, D. J.; Klein, M. L. *Mol. Phys.* **1996**, *87*, 1117–1157.

(60) Kumar, S.; Bouzida, D.; Swendsen, R. H.; Kollman, P. A.; Rosenberg, J. M. *J. Comput. Chem.* **1992**, *13*, 1011–1021.

(61) Asthagiri, D.; Pratt, L. R.; Ashbaugh, H. S. *J. Chem. Phys.* **2003**, *119*, 2702–2708.

(62) Harder, E.; Roux, B. *J. Chem. Phys.* **2008**, *129*, 234706.

(63) Kastenholz, M.; Hunenberger, P. *J. Chem. Phys.* **2006**, *124*, 124106.

(64) Kastenholz, M. A.; Huenenberger, P. H. *J. Chem. Phys.* **2006**, *124*, 224501.

(65) Mahan, G. *Phys. Rev. A* **1980**, *22*, 1780–1785.

(66) Hattig, C.; Hess, B. A. *J. Chem. Phys.* **1998**, *108*, 3863–3870.

(67) Coker, H. *J. Phys. Chem.* **1976**, *80*, 2078–2084.

(68) Coker, H. *J. Phys. Chem.* **1976**, *80*, 2084–2091.

(69) Pyper, N. C.; Pike, C. G.; Edwards, P. P. *Mol. Phys.* **1992**, *76*, 353–372.

(70) Jemmer, P.; Fowler, P. W.; Wilson, M.; Madden, P. A. *J. Phys. Chem. A* **1998**, *102*, 8377–8385.

(71) Džidič, I.; Kebarle, P. *J. Phys. Chem.* **1970**, *74*, 1466–1474.

(72) Tissandier, M. D.; Cowen, K. A.; Feng, W. Y.; Gundlach, E.; Cohen, M. H.; Earhart, A. D.; Coe, J. V.; Tuttle, T. R., Jr. *J. Phys. Chem. A* **1998**, *102*, 7787–7794.

(73) Feller, D.; Glendening, E. D.; Kendall, R. A.; Peterson, K. A. *J. Chem. Phys.* **1994**, *100*, 4981–4997.

(74) Glendening, E. D.; Feller, D. *J. Phys. Chem.* **1995**, *99*, 3060–3067.

(75) Borodin, O.; Bell, R. L.; Li, Y.; Bedrov, D.; Smith, G. D. *Chem. Phys. Lett.* **2001**, *336*, 292–302.

(76) Kim, J.; Lee, H. M.; Suh, S. B.; Majumdar, D.; Kim, K. S. *J. Chem. Phys.* **2000**, *113*, 5259.

(77) Frisch, M. J.; Trucks, G. W.; Schlegel, H. B.; Scuseria, G. E.; Robb, M. A.; Cheeseman, J. R.; Montgomery, J.; Vreven, T.; Kudin, K. N.; Burant, J. C.; Millam, J. M.; Iyengar, S. S.; Tomasi, J.; Barone, V.; Mennucci, B.; Cossi, M.; Scalmani, G.; Rega, N.; Petersson, G. A.; Nakatsuji, H.; Hada, M.; Ehara, M.; Toyota, K.; Fukuda, R.; Hasegawa, J.; Ishida, M.; Nakajima, T.; Honda, Y.; Kitao, O.; Nakai, H.; Klene, M.; Li, X.; Knox, J. E.; Hratchian, H. P.; Cross, J. B.; Bakken, V.; Adamo, C.; Jaramillo, J.; Gomperts, R.; Stratmann, R. E.; Yazyev, O.; Austin, A. J.; Cammi, R.; Pomelli, C.; Ochterski, J. W.; Ayala, P. Y.; Morokuma, K.; Voth, G. A.; Salvador, P.; Dannenberg, J. J.; Zakrzewski, V. G.; Dapprich, S.; Daniels, A. D.; Strain, M. C.; Farkas, O.; Malick, D. K.; Rabuck, A. D.; Raghavachari, K.; Foresman, J. B.; Ortiz, J. V.; Cui, Q.; Baboul, A. G.; Clifford, S.; Cioslowski, J.; Stefanov, B. B.; Liu, G.; Liashenko, A.; Piskorz, P.; Komaromi, I.; Martin, R. L.; Fox, D. J.; Keith, T.; Al-Laham, M. A.; Peng, C. Y.; Nanayakkara, A.; Challacombe, M.; Gill, P. M. W.; Johnson, B.; Chen, W.; Wong, M. W.; Gonzalez, C.; Pople, J. A. *Gaussian 03*, Revision C.02; Gaussian, Inc.: Wallingford, CT, 2004.

(78) Randles, J. *Trans. Faraday Soc.* **1956**, *52*, 1573–1581.

(79) Noyes, R. M. *J. Am. Chem. Soc.* **1962**, *84*, 513–522.

(80) Gomer, R.; Tryson, G. *J. Chem. Phys.* **1977**, *66*, 4413–4424.

(81) Klots, C. E. *J. Phys. Chem.* **1981**, *85*, 3585–3588.

(82) Marcus, Y. *J. Chem. Soc., Faraday Trans.* **1991**, *87*, 2995–2999.

(83) Schmid, R.; Miah, A. M.; Sapunov, V. N. *Phys. Chem. Chem. Phys.* **2000**, *2*, 97–102.

(84) Whitfield, T. W.; Varma, S.; Harder, E.; Lamoureux, G.; Rempe, S. B.; Roux, B. *J. Chem. Theory Comput.* **2008**, *3*, 2068.

(85) Wagman, D. D.; Evans, W. H.; Parker, V. B.; Schumm, R. H.; Halow, I.; Bailey, S. M.; Churney, K. L.; Nuttall, R. L. *J. Phys. Chem. Ref. Data* **1982**, *11*, Supplement No. 2.

(86) Peschke, M.; Blades, A. T.; Kebarle, P. *J. Phys. Chem. A* **1998**, *102*, 9978–9985.

(87) Peschke, M.; Blades, A. T.; Kebarle, P. *J. Am. Chem. Soc.* **2000**, *122*, 10440–10449.

(88) Ohtaki, H.; Radnai, T. *Chem. Rev.* **1993**, *93*, 1157–1204.

(89) Spangberg, D.; Rey, R.; Hynes, J. T.; Hermansson, K. *J. Phys. Chem. B* **2003**, *107*, 4470–4477.

(90) Varma, S.; Rempe, S. B. *Biophys. Chem.* **2006**, *124*, 192–199.

(91) Lyubartsev, A. P.; Laasonen, K.; Laaksonen, A. *J. Chem. Phys.* **2001**, *114*, 3120–3126.

(92) Todorova, T.; Hunenberger, P. H.; Hutter, J. *J. Chem. Theory Comput.* **2008**, *4*, 779–789.

(93) Caminiti, R.; Licheri, G.; Piccaluga, G.; Pinna, G. *Chem. Phys. Lett.* **1977**, *47*, 275–278.

(94) Martinez, J. M.; Pappalardo, R. R.; Marcos, E. S. *J. Am. Chem. Soc.* **1999**, *121*, 3175–3184.

(95) *CRC Handbook of Chemistry and Physics*, 87th ed.; Lide, D. R., Ed.; Taylor and Francis: Boca Raton, FL, 2007.

(96) Roux, B. *Biophys. J.* **1996**, *71*, 3177–3185.

(97) Harder, E.; Anisimov, V. M.; Vorobyov, I. V.; Lopes, P. E. M.; Noskov, S. Y.; MacKerell, A. D., Jr.; Roux, B. *J. Chem. Theory Comput.* **2006**, *2*, 1587–1597.

(98) Luo, Y.; Roux, B. *J. Phys. Chem. Lett.* **2010**, *1*, 183–189.